

Low-temperature structure and the ferroelectric phase transitions in the CdTiO₃ perovskiteBrendan J. Kennedy,^{1,*} Qingdi Zhou,¹ Shipeng Zhao,² Fanhao Jia,² Wei Ren,^{2,†} and Kevin S. Knight^{3,4}¹*The School of Chemistry, The University of Sydney, Sydney NSW 2006, Australia*²*Physics Department and International Centre for Quantum and Molecular Structures, Shanghai University, Shanghai 200444, China*³*Department of Earth Sciences, University College London, Gower Street, London WC1E 6BT, United Kingdom*⁴*Department of Earth Sciences, The Natural History Museum, Cromwell Road, London SW7 5BD, United Kingdom*

(Received 16 July 2017; revised manuscript received 9 November 2017; published 13 December 2017)

The paraelectric-ferroelectric transition in CdTiO₃ has been monitored using high-resolution neutron diffraction data. This necessitated preparing a sample enriched in ¹¹⁴Cd. A subtle, but significant, anisotropy in the thermal expansion of the lattice parameters for CdTiO₃ associated with the transition to the polar structure was observed. First-principles calculations are presented to understand energies, phonon dispersion, and structures of possible phases with different symmetries.

DOI: [10.1103/PhysRevB.96.214105](https://doi.org/10.1103/PhysRevB.96.214105)**I. INTRODUCTION**

Titanium-containing perovskites play a critical, if not always widely appreciated, role in many modern electronic devices. The importance of PbZr_{1-x}Ti_xO₃ (PZT) $x \sim 0.48$ is well documented [1] and PZT ceramics are the most widely employed materials for piezoelectric actuators used in disk drives, motion sensors and controllers, optics and photonics, to name but a few applications. PbTiO₃-based epitaxial superlattices can also be grown at atomistic levels, which provides designs for new electronic devices made from oxide interfaces [2]. Barium titanate (BaTiO₃) is equally pervasive, being commonly employed as a dielectric ceramic capacitor used in, e.g., wireless local area networks and other frequency-dependent applications [3]. Other titanium perovskites have more specialized applications, e.g., strontium titanate (SrTiO₃) is used in varistors and in tunable high-temperature superconductor microwave filters [4]; it is also of interest for use as an anode in lithium ion batteries [5]. Layered titanates such as Bi₄Ti₃O₁₂ are of interest for use in ferroelectric random access memory [6]. EuTiO₃ thin films might be transformed to a ferroelectric ferromagnet through strain engineering resulting in a multiferroic material [7].

The attractive physical properties of these titanates are related to their crystal structures and it is not surprising that a vast body of information exists for these oxides [8]. SrTiO₃ has a tolerance factor of 1.002, defined as $t = (R_A + R_O)/\sqrt{2}(R_B + R_O)$ where R_A , R_B , and R_O are the relative ionic radii of the 12-coordinate *A*-site and six-coordinate *B*-site cations and the oxygen ion, respectively [9]. As expected for a perovskite with $t \sim 1$ SrTiO₃ adopts the ideal cubic perovskite structure at room temperature. However, cooling SrTiO₃ below 105 K results in an antiferrodistortive transition to a tetragonal phase in which the corner-sharing TiO₆ octahedra are rotated in opposite senses in neighboring unit cells. This is associated with a softening of a single component of the triply degenerate R_4^+ mode [10]. Further cooling results in a softening of the ferroelectric polar phonons, Γ_4^- modes, and although these appear to extrapolate to a

ferroelectric transition close to 20 K, the softening saturates and no such transition is observed [11].

The Sr²⁺ (ionic radii 1.44 Å) cations in SrTiO₃ can be replaced by larger Ba²⁺ (1.61 Å [9]) cations increasing the tolerance factor to 1.061. At high temperatures BaTiO₃ is isostructural with cubic SrTiO₃; however, cooling below 405 K results in a transition to a tetragonal phase in space group *P4mm*. The tetragonal phase is ferroelectric with spontaneous polarization due to the noncentrosymmetric displacement of Ti⁴⁺ and O²⁻ ions relative to the Ba²⁺ ions. Upon further cooling bulk BaTiO₃ undergoes two more phase transformations, from the tetragonal ferroelectric phase to an orthorhombic ferroelectric phase at 278 K and then to the rhombohedral ferroelectric phase below 185 K, although recent studies suggest a monoclinic phase may also exist [12,13].

PbTiO₃, like BaTiO₃, is tetragonal and ferroelectric at room temperature [14]. This is consistent with the relative size of the cations; Pb²⁺ being slightly larger than Sr²⁺, 1.49 vs 1.44 Å resulting in a slightly larger tolerance factor of $t = 1.019$ for PbTiO₃. Surprisingly PbTiO₃ has a larger tetragonal distortion and higher Curie temperature than BaTiO₃, 763 vs 405 K [15]. While early studies concluded [16] that PbTiO₃ is a typical displacive ferroelectric, there is some experimental evidence for order-disorder behavior in this material as a consequence of the Pb stereochemically active lone pair 6s electrons which makes Pb²⁺ more deformable and polarizable than Ba²⁺ or Sr²⁺ [17]. The increased covalent character of Pb compared to Ba or Sr is believed to be important in stabilizing the relatively high Curie temperature of PbTiO₃.

Conversely replacing Sr²⁺ with smaller Ca²⁺ (1.34 Å) cations introduces cooperative tilting of the TiO₆ octahedra resulting in an orthorhombic structure at room temperature [18]. The cubic CaTiO₃ structure (which is experimentally realized above 1390 K [19]) has an unstable polar Γ_4^- mode that, if frozen, would yield a ferroelectric phase with nonzero net polarization. That fact that this mode does not contribute to bulk CaTiO₃ has led to the suggestion that TiO₆ tilting (from the R_4^+ and M_3^+ modes) inhibits it [20]. Dielectric measurements have suggested that CaTiO₃, like SrTiO₃, is an incipient ferroelectric at low temperatures [21].

Compared to the above ATiO₃ (*A* = Ca, Sr, Ba, Pb) oxides relatively little is known about CdTiO₃. CdTiO₃ can be obtained with either an ilmenite or perovskite-type structure [22].

*brendan.kennedy@sydney.edu.au

†renwei@shu.edu.cn

Cd^{2+} (1.31 Å) is slightly smaller than Ca^{2+} (1.34 Å) giving a similar tolerance factor, 0.955 vs 0.966; however, Cd is generally regarded as being more polarizable than Ca as a consequence of the filled $4d$ shell. Kay and Miles [23] proposed a ferroelectric structure for perovskite-type CdTiO_3 at room temperature in space group $Pc2_1n$ (an alternate setting of space group 33, $Pna2_1$), whereas Sasaki *et al.* [18] concluded it was nonpolar in $Pnma$ (space group 62), and hence isostructural with CaTiO_3 [19]. *Ab initio* calculations show the nonpolar $Pnma$ structure to be stable. Nevertheless, it has been demonstrated that CdTiO_3 undergoes a displacive ferroelectric phase transition at about 80 K [24] and that there is potential to tune T_C by substitution of other cations at the A -site position as illustrated by studies of $\text{Cd}_{1-x}\text{Ca}_x\text{TiO}_3$ [25]. Recent x-ray diffraction studies have confirmed that the room-temperature paraelectric phase is in $Pnma$ and have suggested the low-temperature ferroelectric phase is in either $Pna2_1$ [24] or $P2_1ma$ [26]. Our present work favors the $Pna2_1$ structure in which the Γ_4^- mode condenses [22] and *ab initio* calculations show that the polar $Pna2_1$ structure is more stable than the nonpolar $Pnma$ structure. The structure of the ferroelectric phase of CdTiO_3 is of interest since the TiO_6 octahedron is well known for its tendency to form polar groups where the Ti is displaced from the geometrical center of the surrounding oxygen atoms. The octahedral rotations [27] in CaTiO_3 and CdTiO_3 have a similar magnitude at room temperature and a comparison of the low-temperature behavior of these two oxides is likely to be informative regarding the competition between cation displacement and octahedral tilting.

In the present work we have utilized high-resolution neutron diffraction ($\Delta d/d = 6 \times 10^{-4}$, to first order independent of Q , $Q = 4\pi \sin(\theta)/\lambda$) to study the structural changes that accompany the paraelectric-ferroelectric transition in CdTiO_3 since neutron diffraction is expected to provide a more accurate and precise description of these structures compared with x-ray diffraction methods. To overcome the high neutron absorption cross section of naturally occurring Cd we used a sample enriched in ^{114}Cd [28].

II. EXPERIMENT

^{114}CdO (~ 0.7 g; Isoflex 99.8% isotope purity) was used as supplied and TiO_2 (Aldrich 99.9 + %) was preheated at 1000 °C for 12 h before use. A stoichiometric mixture of the two oxides, sufficient to form 1.0 g of product, was mixed by hand and heated at 700 °C for 12 h. After regrinding, the powder sample was pressed into a pellet and heated first at 800 °C for 60 h and then at 950 °C for 45 h [22].

The polycrystalline CdTiO_3 sample was loaded into an aluminum sample can of slab geometry with thin, neutron-transparent, vanadium windows. The sample container houses a 100 W cartridge heater inserted into one wall and a Rh-Fe sensor inserted into the opposite wall. Thermal contact between the sample container, heater, and the sensor was achieved using a copper-based antiseize compound. A neutron-absorbing, gadolinium mask was attached to the side of the can facing the incident beam and backscattering detectors to prevent contaminant Bragg peaks arising from either the

body of the sample can, including the sensor and heater, or the stainless-steel frames supporting the vanadium windows. For the low-temperature measurement the assembly was mounted in a Sumitomo RDK-415D top-loading closed-cycle refrigerator (CCR) under 30 mbar of helium exchange gas.

Data were collected at 9, 15, and 20 K and then in 10 K steps to 60 K and 5 K steps to 100 K. After this the sample was heated to 300 K and a smaller number of patterns were recorded as the sample was recooled to 90 K, at 267, 133, 100, 167, 133, and 100 K. The data at 9 and 300 K were measured for 120 Ah incident proton beam current, while the other measurements were made for 40 Ah, approximately 60 min duration. Once the control sensor had reached the set point temperature, data collection was commenced after a 3 min thermal equilibration period; thermal stability was of the order ± 0.2 K for all data collection temperatures.

The neutron time-of-flight data were focused (summation of individual detector elements onto a common d -spacing scale), normalized to the incident flux distribution and corrected for self-shielding and wavelength-dependent absorption. Data in the time-of-flight range 32–120 ms, corresponding to a d -spacing range of ~ 0.64 – 2.4 Å, were analyzed using the GSAS package [29].

III. COMPUTATIONAL METHOD

The *ab initio* structural relaxations and energy calculations were performed using density functional theory (DFT) within the strongly constrained and appropriately normed (SCAN) semilocal density functional [30,31] metageneralized gradient approximation as implemented in the VASP package [32]. For the geometry optimization, an energy cutoff of 600 eV for the plane-wave basis set and Monkhorst-Pack Brillouin [33] zone sampling grid with the resolution of $2\pi \times 0.03 \text{ \AA}^{-1}$ was used, to ensure that enthalpy calculations are well converged to better than 1 meV per atom. The phonon dispersions were computed based on the supercell approach using the PHONOPY [34,35] code interfaced with the density functional perturbation theory [36]. A $2 \times 2 \times 2$ cubic superlattice (8 Cd atoms, 8 Ti atoms and 24 O atoms) was used in the phonon calculations for the $Pm\bar{3}m$ phase, a $2 \times 2 \times 1$ superlattice (16 Cd atoms, 16 Ti atoms, and 48 O atoms) was used in the calculations for the $Pna2_1$ and $Pnma$ phases, and a $2 \times 2 \times 2$ superlattice (16 Cd atoms, 16 Ti atoms, and 48 O atoms) for the $R\bar{3}$ phase.

IV. RESULTS AND DISCUSSION

Potential structures for CdTiO_3 were fully optimized and the calculated lattice parameters as well as total energy values at ambient pressure are listed in Table I. The calculated lattice parameters of $Pnma$ - CdTiO_3 and $Pna2_1$ - CdTiO_3 are very similar to previous estimates [38].

It can be clearly seen that crystallographically observed structures of CdTiO_3 (see Fig. 1) are much more energetically favorable than the archetypal cubic perovskite $Pm\bar{3}m$ phase, and the $R\bar{3}$ ilmenite-type structure is found to be the most stable phase at ambient pressure as it has lowest energy at its equilibrium lattice constants. This is consistent with the results from Table I. To investigate the dynamic stability, the phonon

TABLE I. Optimized equilibrium lattice parameters a , b , and c (Å); relative energy per formula unit (meV/f.u.) at ambient pressure of CdTiO₃ with different space groups by SCAN functional. The data in parentheses are the local-density approximation results.

Space group	a (Å)	b (Å)	c (Å)	Energy (meV/f.u.)
$Pm\bar{3}m$ (221)	3.85 (3.81)	3.85 (3.81)	3.85 (3.81)	405.8 (1033.8)
$I4/mcm$ (140)	5.37 (5.32)	5.37 (5.31)	7.69 (7.61)	125.5 (279.8)
$P4/mbm$ (127)	5.38 (5.32)	5.38 (5.32)	3.85 (3.81)	124.4 (271.8)
$I4/mmm$ (139)	7.66 (7.59)	7.66 (7.59)	7.56 (7.47)	76.4 (165.5)
$Im\bar{3}$ (204)	7.63 (7.56)	7.63 (7.56)	7.63 (7.56)	70.9 (156.5)
$Cmcm$ (63)	7.56 (7.49)	7.64 (7.57)	7.65 (7.58)	45.4 (99.4)
$Imma$ (74)	5.49 (5.45)	7.58 (7.50)	5.33 (5.27)	38.0 (83.9)
$C2/c$ (15)	9.36 (9.16)	5.55 (5.45)	9.36 (10.54)	35.5 (76.8)
$R\bar{3}c$ (167)	5.36 (5.32)	5.36 (5.32)	13.39 (13.23)	35.5 (86.3)
$Pnma$ (62)	5.44 (5.38)	7.62 (7.56)	5.31 (5.25)	0.14 (0.24)
	5.40 (Ref. [34])	7.59	5.28	
$P2_1ma$ (26)	5.44 (5.38)	7.63 (7.56)	5.32 (5.25)	0.14 (0.24)
$Pna2_1$ (33)	5.43 (5.38)	7.65 (7.56)	5.31 (5.25)	0
	5.40 (Ref. [34])	7.58	5.31	
$R\bar{3}$ (138)	5.25 (5.50)	5.25 (5.20)	14.91 (14.66)	-64.4 (-100.9)
	5.24 (Ref. [37])	5.24	14.84	

Note that in Ref. [34] a nonconventional setting $\sqrt{2}a \times 2a \times \sqrt{2}a$ has been used.

dispersions were calculated for selected phases of CdTiO₃, as shown in Fig. 2. The phonon spectrum of the $Pnma$ and $Pna2_1$ phases in our calculations are dynamically stable. However, we can see that the two modes softening at the Γ point in the paraelectric $Pnma$ phase may still indicate the possibility of some kind of instability with ferroelectric phase transition. So we calculated the phonon spectrum of the $Pnma$ phase with 1% expansion of volume, which indicates those two modes softening corresponds to this instability. Combined with our DFT calculations and AMPLIMODES [39] analysis, we found that these two modes are one 7-dimensional nonpolar mode Γ_1^+ (isotropy subgroup $Pnma$) and one 8-dimensional polar mode Γ_4^- (isotropy subgroup $Pna2_1$), with amplitudes found to be 0.0478 Å and 0.3427 Å, respectively, indicating that the latter is the primary distortion mode, consistent with our previous discussion of experiment observations [22].

The sample of ¹¹⁴CdTiO₃ used in this work was prepared using conventional solid-state methods. The use of ¹¹⁴Cd is essential in order to overcome the high neutron absorption cross section of naturally occurring Cd. The neutron diffraction pattern for this sample, recorded at room temperature (Fig. 3), was well fitted in space group $Pnma$ with $\chi^2 = 2.15\%$, and other than some weak reflections, most probably vanadium from the CCR windows, all the peaks were accounted for by the structural model. The refined lattice parameters of $a = 5.42162(3)$, $b = 7.61860(4)$, and $c = 5.30663(3)$ Å are in excellent agreement with earlier studies [18,22]. This corresponds to a $\sqrt{2}a_p \times 2a_p \times \sqrt{2}a_p$ supercell of the basic cubic perovskite cell in which a_p , the idealized perovskite lattice parameter, is ~ 3.8 Å. The larger cell is a consequence of the cooperative tilting of the corner-sharing TiO₆ octahedra. The unit cell contains four formula units of CdTiO₃. The

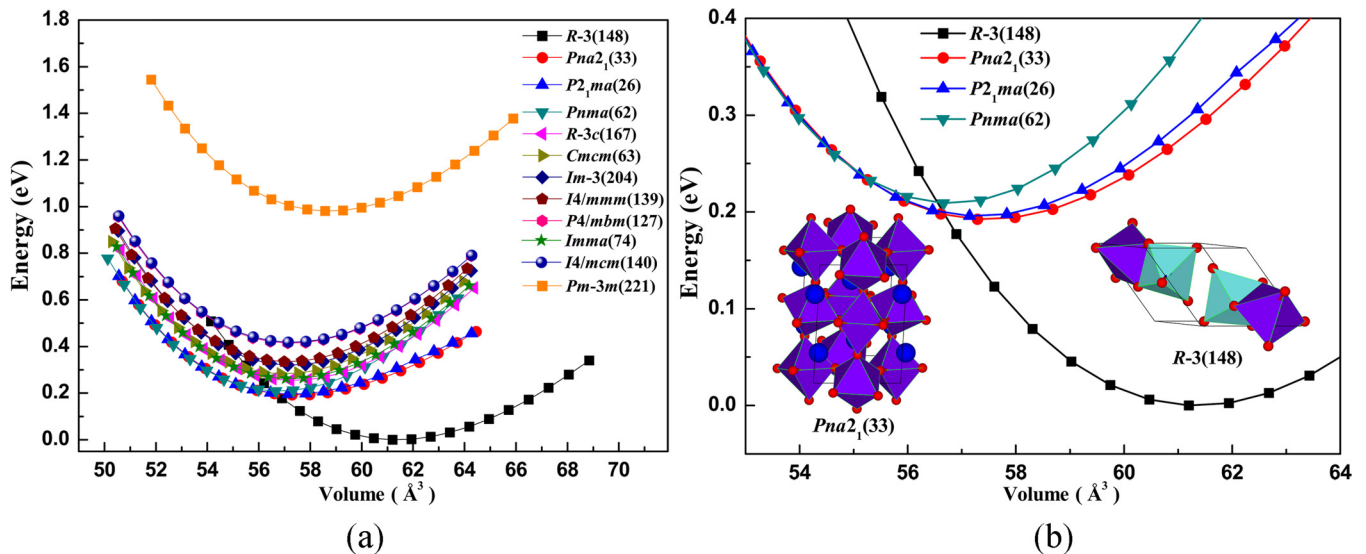


FIG. 1. The total energy versus f.u. volume for CdTiO₃ with different space groups. From the 12 structures in panel (a) the four low-energy phases are highlighted in panel (b).

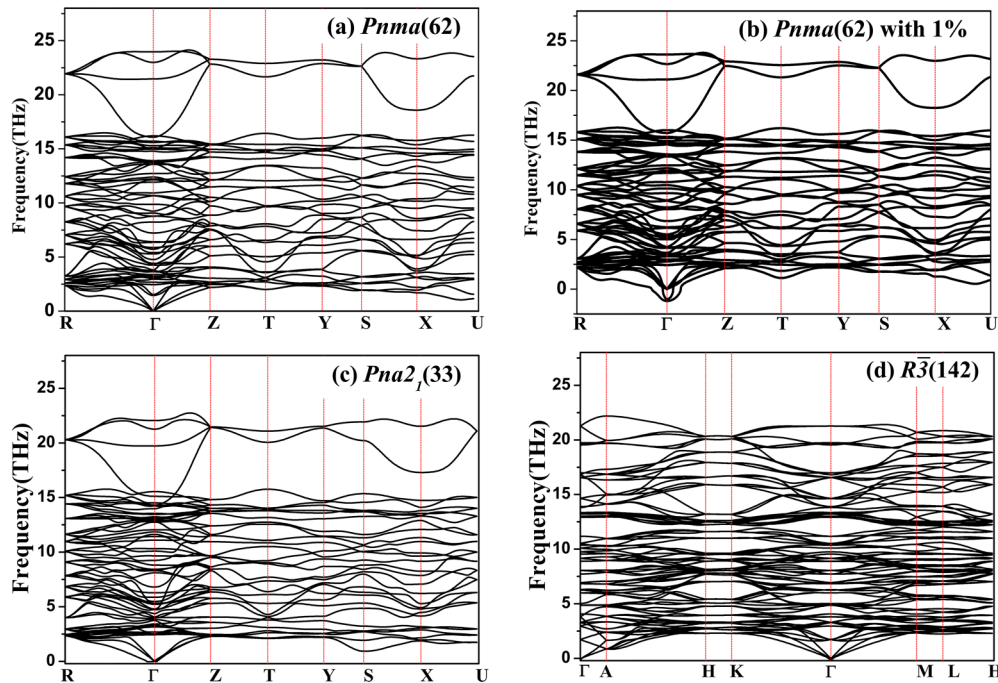


FIG. 2. Phonon dispersion curves for the (a) $Pnma$ phase, (b) $Pnma$ phase with 1% expansion of volume, (c) $Pn2_1a$ phase and (d) $R\bar{3}$ phase of $CdTiO_3$.

orthorhombic $Pnma$ structured phase is obtained from the ideal cubic $Pm\bar{3}m$ structure by a combination of the two independent octahedral tilts in $CdTiO_3$, ψ and φ , where ψ is an antiphase tilt about the pseudocubic $\langle 101 \rangle_p$ axes, and φ is an in-phase tilt about the pseudocubic $\langle 010 \rangle_p$ axis. This is described as $a^-b^+a^-$ following Glazer's notation [40] where negative or out-of-phase tilts are due to the condensation of the R_4^+ modes and the positive or in-phase tilts arise from the M_3^+ modes [27]. The magnitudes of the tilts were estimated from the atomic coordinates refined from powder neutron diffraction data [41]. We find $\psi = 14.7(2)^\circ$ and $\varphi = 10.6(2)^\circ$.

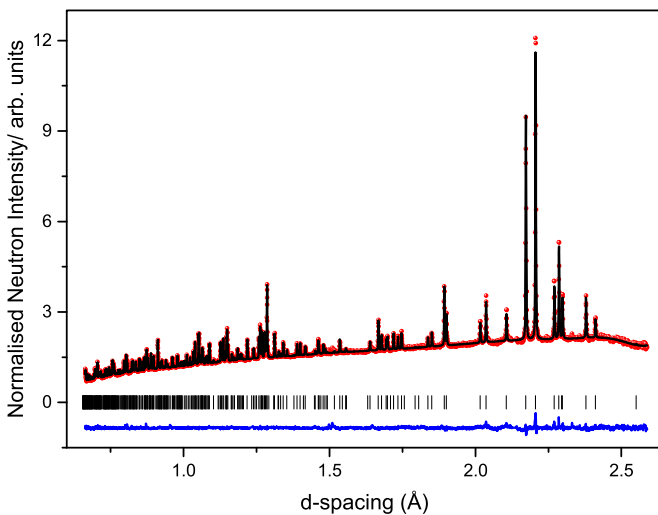


FIG. 3. Observed, calculated and difference neutron diffraction profile for $CdTiO_3$. The data were recorded at 300 K and fit is in space group $Pnma$ to the parameters listed in Table II.

These values are somewhat larger than those estimated for $CaTiO_3$ at the same temperature, $11.1(2)^\circ$ and $9.0(2)^\circ$. The tilts do not, however, provide any information regarding local displacements of the atoms and/or distortion of the TiO_6 octahedra; this information is given by the secondary modes which were estimated using the program AMPLIMODES. The modes of symmetry R_4^+ and M_3^+ are observed to have the largest magnitudes. At 300 K the magnitude of the R_4^+ mode was 1.409(3) and that of the M_3^+ mode was 1.025(3). These values were essentially identical at 100 K, 1.418(5) and 1.024(6). By way of comparison for $CaTiO_3$ at 300 K, the values were 1.116 and 0.854 and at 100 K the values were 1.143 and 0.863. The magnitude of these indicate that upon heating the in-phase tilts will probably be lost first in both oxides, and this will occur at higher temperatures in $CdTiO_3$ than in $CaTiO_3$.

Additional smaller modes are generated through anharmonic coupling with the two fundamental unstable tilting modes; the most important of these is the X_5^+ mode. This distortion is two dimensional, in the sense that it involves two basis symmetry modes, one for the Cd atoms and another for the oxygen anions, and produces a distortion of the octahedron. The magnitude of the X_5^+ mode in $CdTiO_3$ was 0.516(2) and 0.534(4) at 300 and 100 K, respectively. Although the TiO_6 octahedra in $CdTiO_3$ are distorted, the three Ti-O distances are all very similar: Ti-O(1), 1.9705(4); Ti-O2a, 1.9620(10); Ti-O2b, 1.9665(11) Å with the average Ti-O distance of 1.966 Å being comparable to that seen in $CaTiO_3$ [18,19]. The structure is illustrated in Fig. 4.

The larger Cd^{2+} cations occupy the perovskite cuboctahedral sites, although as a consequence of the tilting of the TiO_6 octahedra the Cd^{2+} cations are effectively eight coordinate with the other four Cd-O contacts being greater than 3.1 Å. The bond valence sum for the Ti cation is 3.97, while that for

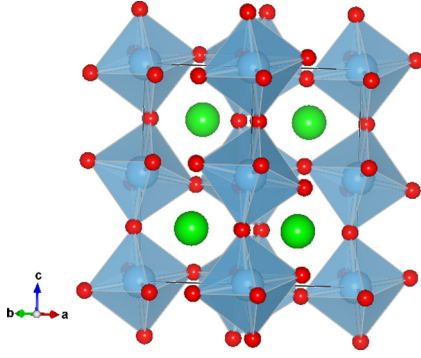


FIG. 4. Representation of the corner-sharing TiO_6 arrangement in CdTiO_3 . The Ti cations are represented by gray spheres at the center of the octahedra. The oxygen atoms are represented by the small red spheres and the Cd cations by the green spheres.

the Cd cation is 1.66 showing this is slightly underbonded. The refined structural parameters for the perovskite-type CdTiO_3 structure are collected in Table II.

Despite the observation of ferroelectric properties below around 80 K in CdTiO_3 , demonstrating that the low-temperature structure must be in a polar, noncentrosymmetric space group, cooling the sample to 8 K did not result in the appearance of any new reflections in the neutron diffraction pattern, nor was any additional splitting of either the strongest Bragg or weaker superlattice reflections evident. The cell was clearly still orthorhombic and a satisfactory fit was obtained in $Pnma$ with $\chi^2 = 2.73\%$. Note that the space groups derived from symmetry descent from space group $Pnma$ via the polar modes Γ_2^- (space group $Pnm2_1$), Γ_3^- (space group $P2_1ma$), and Γ_4^- (space group $Pn2_1a$) are in distinguishable on systematic absence conditions. The atomic displacement parameters for each of the ions were unexceptional, although attempts to refine anisotropic displacement parameters resulted in physically implausible values. This situation is similar to that reported recently by Belik *et al.* [42] who observed that attempting to refine the structure of BiInO_3 in a nonpolar space group resulted in unusual displacement parameters. These workers concluded that for BiInO_3 it was not possible to distinguish between nonpolar $Pnma$ and

TABLE II. Crystal structure data and refined atomic coordinates and atomic displacement parameters (10^{-2} \AA^2) for perovskite-type CdTiO_3 at room temperature in space group $Pnma$.

Name	Site	x	y	z	U_e^*		
Cd	4c	0.5390(3)	$\frac{1}{4}$	0.0082(3)	1.14*		
Ti	4a	0	0	0	0.96*		
O1	4c	-0.0280(3)	$\frac{1}{4}$	-0.0908(3)	1.03*		
O2	8d	0.2964(2)	0.0473(1)	0.2009(2)	1.13*		
		U_{11}	U_{22}	U_{33}	U_{12}	U_{13}	U_{23}
Cd		1.12(6)	1.03(7)	1.28(7)	0	0.38(7)	0
Ti		0.81(12)	1.00(10)	1.08(9)	0.24(7)	-0.33(10)	0.39(9)
O1		1.49(8)	0.58(7)	1.02(7)	0	-0.03(6)	0
O2		0.96(4)	1.34(5)	1.09(4)	-0.06(4)	-0.11(5)	0.05(5)

*Isotropic equivalent values.

TABLE III. Crystal structure data and refined atomic coordinates and atomic displacement parameters (10^{-2} \AA^2) for CdTiO_3 at 8 K in space group $Pn2_1a$. $a = 5.41579(3)$, $b = 7.60230(4)$, $c = 5.29487(3) \text{ \AA}$. The y parameter of the Ti cation has been fixed at 0 to define the origin.

Name	Site	x	y	z	U_e
Cd	4a	0.4597(3)	0.2446(12)	0.0092(3)	0.63(3)
Ti	4a	-0.0140(11)	0	-0.0080(13)	0.39(5)
O1	4a	0.5285(2)	0.2476(14)	0.5911(2)	0.81(3)
O2	4a	0.2036(12)	0.0416(11)	0.2968(12)	1.05(12)
O3	4a	-0.2006(11)	-0.0545(11)	-0.3006(10)	0.52(3)

the polar $Pna2_1$ structures as a consequence of the large displacement ($\sim 0.25 \text{ \AA}$) of the heavy Bi^{3+} ions from the mirror plane [42].

In the present case the fit in $Pna2_1$ was comparable to that obtained in $Pnma$ $\chi^2 = 2.69$ vs 2.73% and careful examination of the neutron diffraction data failed to reveal any features that could be used to distinguish between the two possibilities, even though the displacement of the Cd^{2+} in CdTiO_3 shows a similarly large displacement ($\sim 0.22 \text{ \AA}$) to that of the Bi in BiInO_3 . Nevertheless, since CdTiO_3 must have a noncentrosymmetric structure at low temperature, space group $Pna2_1$ is preferred. As shown in Table I, the energy of this is slightly lower than that of the nonpolar $Pnma$ phase and the final refined parameters for this at 8 K are given in Table III.

The distortion of the low-temperature ferroelectric $Pn2_1a$ phase with respect to the parent $Pnma$ modification was explored in terms of symmetry-adapted modes. The $Pn2_1a$ distortion can be described by two modes corresponding to the irreducible representations Γ_1^+ and Γ_4^- . The amplitudes of the nonpolar Γ_1^+ (isotropy subgroup $Pnma$) and polar Γ_4^- (isotropy subgroup $Pn2_1a$) were found to be 0.0377 and 0.1889 \AA , respectively, indicating that the latter is the primary distortion mode.

The thermal expansion of the unit cell of perovskite-structured phases is most easily appreciated by examining the pseudocubic subcell metric, which in the case of space group $Pnma$ is monoclinic with $a_{pc} = c_{pc} \neq b_{pc}$, $\beta_{pc} \neq 90^\circ$. This temperature variation is illustrated in Fig. 5 where the ferroelectric-paraelectric transition is immediately evident from the anomalies in both the unit-cell edges and the monoclinic shear angle. The a_{pc} (equivalent c_{pc}) shows no evidence for a low-temperature saturation region, immediately reducing with increasing temperature toward the ferroelectric transition temperature, i.e., negative linear thermal expansion along a_{pc} and c_{pc} indicating the presence of modes with negative Grüneisen parameters, while b_{pc} behaves in a more conventional manner at low temperatures but exhibits a near discontinuity in its linear thermal expansion coefficient $\pm 10 \text{ K}$ of the transition temperature. The behavior of the shear angle is also a complex function of temperature exhibiting no saturation at low temperature and a discontinuity in its temperature derivative at the ferroelectric-paraelectric transition temperature. This figure demonstrates the coupling of the polar displacement with the lattice and illustrates the advantage of

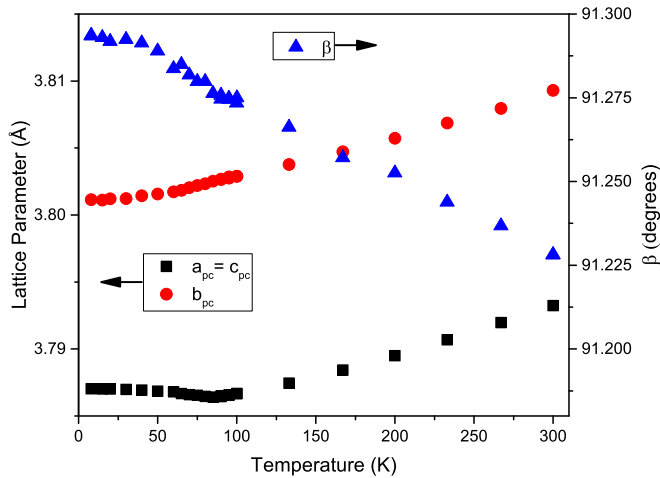


FIG. 5. Temperature dependence of the pseudocubic lattice parameters of CdTiO_3 between 7 and 300 K (transformation from orthorhombic to pseudocubic cell $1/2\ 0\ 1/2/0\ 1/2\ 0/-1/2\ 0\ 1/2$). The estimated standard deviations are less than the size of the symbols. The pseudocubic volume is simply $\frac{1}{2}$ of the unit-cell volume which is illustrated in Fig. 6.

the high-resolution diffraction, which provides precise and accurate lattice parameters, in identifying this.

The unit-cell volume, illustrated in Fig. 6, shows weak evidence of negative volume expansivity below the phase transition temperature and an extended region of ultralow thermal expansion below 100 K. From our DFT calculation (SCAN functional fits very well with experiment in the volume calculation), the ground state of the $Pna2_1$ phase ($220.575\ \text{\AA}^3/\text{f.u.}$) has bigger volume than the $Pnma$ phase ($220.114\ \text{\AA}^3/\text{f.u.}$), which indicates the possibility of negative thermal volumetric expansion. The highly anomalous unit-cell

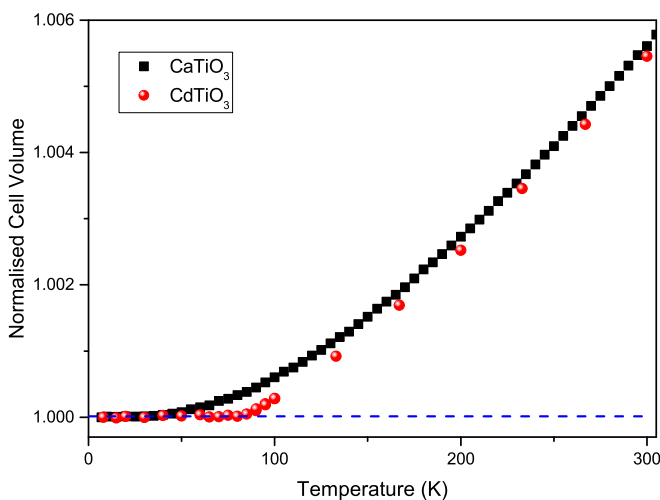


FIG. 6. Temperature dependence of the normalized cell volume [Volume(T)/Volume(0 K)] of CdTiO_3 (closed symbols) and CaTiO_3 (open symbols). Estimated standard deviations for the unit-cell volumes are substantially smaller than the plotting symbols for both phases at all temperatures. The data for CaTiO_3 are taken from Knight [43].

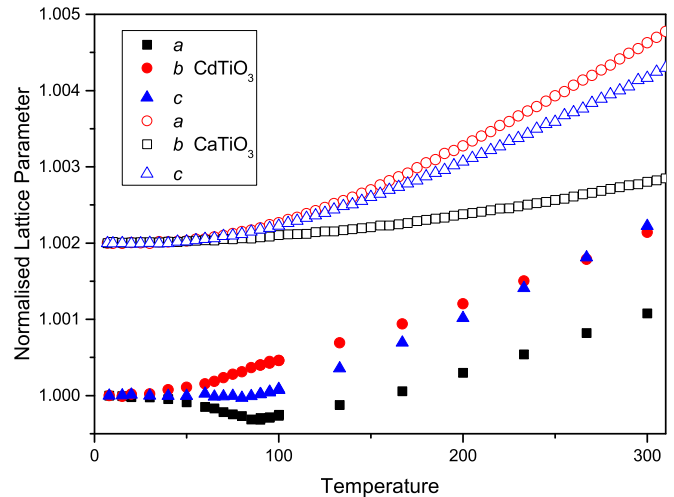


FIG. 7. Temperature dependence of the normalized lattice parameters of CdTiO_3 (closed symbols) and CaTiO_3 (open symbols). The values for CaTiO_3 have been offset for clarity. The data for CaTiO_3 are taken from Knight [43] transformed to $Pnma$. Estimated standard deviations for the unit-cell volumes are substantially smaller than the plotting symbols for both phases at all temperatures.

behavior of CdTiO_3 is most easily appreciated by comparing its behavior with the nonferroelectric compound CaTiO_3 , as shown in Figs. 6 and 7. Despite showing incipient ferroelectric behavior, the unit-cell volume of CaTiO_3 behaves in a conventional manner with a low-temperature saturation region only extending to 40–50 K in comparison with the near 100 K region in CdTiO_3 . Despite this low-temperature volume expansivity, by 150 K the volume expansion coefficient of CdTiO_3 is approaching that of CaTiO_3 , and above 200 K, the two compounds have very similar temperature dependence.

Unfortunately, the extreme mass difference between Ca and Cd precludes using the low-temperature unit-cell data of CaTiO_3 as a baseline for a calculation of the spontaneous strains in CdTiO_3 below the ferroelectric-paraelectric phase transition.

V. CONCLUSION

A perovskite-type phase of CdTiO_3 can be prepared at low temperatures which irreversibly transforms to a rhombohedral ($R\bar{3}$) ilmenite-structured phase [22]. First-principles calculations confirm that this rhombohedral is the most stable structure for CdTiO_3 at 0 GPa, consistent with experimental observations. Considering the metastable perovskite-type phase, first-principles calculations show that the energy difference between the polar $Pn2_1a$ and nonpolar $Pnma$ - CdTiO_3 structures is small and both of them are dynamically stable. The exceptional precision available through analysis of neutron diffraction data obtained from the high-resolution powder diffractometer has allowed the paraelectric-ferroelectric transition in perovskite-type CdTiO_3 to be followed. It has been established that the lattice parameters of perovskites are sensitive to effects such as octahedral tilting, Jahn-Teller distortion, and magnetostriction [44]. In the present work we observe a subtle, but significant, anisotropy in the thermal

expansion of the lattice parameters for CdTiO₃ associated with the transition to the polar structure.

ACKNOWLEDGMENTS

B.J.K. acknowledges the support of the Australian Research Council and the Australian Institute of Nuclear Science and Engineering for their support of aspects of this work. This work

was also supported by the National Natural Science Foundation of China (Grants No. 51672171 and No. 11274222), the National Key Basic Research Program of China (Grant No. 2015CB921600), and the Eastern Scholar Program from the Shanghai Municipal Education Commission. The Special Program for Applied Research on Super Computation of the NSFC-Guangdong Joint Fund (the second phase) and Shanghai Supercomputer Center are also acknowledged.

-
- [1] B. Jaffe, W. R. Cook, and H. Jaffe, *Piezoelectric Ceramics* (Academic Press, New York, 1971).
- [2] Y. R. Yang, M. Stengel, W. Ren, X. H. Yan, and L. Bellaiche, *Phys. Rev. B* **86**, 144114 (2012).
- [3] F. Jona and G. Shirane, *Ferroelectric Crystals* (Dover, New York, 1993).
- [4] J. Li, S. Li, and M. A. Alim, *J. Mater. Sci.: Mater. Electron.* **17**, 503 (2006).
- [5] D. C. Johnson and A. L. Prieto, *J. Power Sources* **196**, 7736 (2011).
- [6] B. H. Park, S. J. Hyun, S. D. Bu, T. W. Noh, J. Lee, H.-D. Kim, T. H. Kim, and W. Jo, *Appl. Phys. Lett.* **74**, 1907 (1999).
- [7] Y. R. Yang, W. Ren, D. W. Wang, and L. Bellaiche, *Phys. Rev. Lett.* **109**, 267602 (2012).
- [8] R. H. Mitchell, *Perovskites: Modern and Ancient* (Almaz Press, Thunder Bay, Canada, 2003).
- [9] R. D. Shannon, *Acta Cryst.* **A32**, 751 (1976).
- [10] G. Shirane and Y. Yamada, *Phys. Rev.* **177**, 858 (1969).
- [11] J. Han, F. Wan, Z. Zhu, and W. Zhang, *Appl. Phys. Lett.* **90**, 031104 (2007).
- [12] P. V. Balachandran, D. Z. Xue, and T. Lookman, *Phys. Rev. B* **93**, 144111 (2016).
- [13] Y. J. Gu, F. Xue, S. M. Lei, T. T. A. Lummen, J. J. Wang, V. Gopalan, and L. Q. Chen, *Phys. Rev. B* **90**, 024104 (2014).
- [14] G. Shirane, R. Pepinsky, and B. C. Frazer, *Acta Cryst.* **9**, 131 (1956).
- [15] G. A. Rossetti and N. Maffei, *J. Phys.: Condens. Matter* **17**, 3953 (2005).
- [16] A. M. Glazer and S. A. Mabud, *Acta Cryst.* **B34**, 1065 (1978).
- [17] J. Frantti, *J. Phys. Chem. B* **112**, 6521 (2008).
- [18] S. Sasaki, C. T. Prewitt, J. D. Bass, and W. A. Schulze, *Acta Cryst.* **C43**, 1668 (1987).
- [19] B. J. Kennedy, C. J. Howard, and B. C. Chakoumakos, *J. Phys.: Condens. Matter* **11**, 1479 (1999).
- [20] C. J. Eklund, C. J. Fennie, and K. M. Rabe, *Phys. Rev. B* **79**, 220101 (2009).
- [21] V. V. Lemanov, A. V. Sotnikov, E. P. Smirnova, M. Weihnacht, and R. Kunze, *Solid State Commun.* **110**, 611 (1999).
- [22] B. J. Kennedy, Q. D. Zhou, and M. Avdeev, *J. Solid State Chem.* **184**, 2987 (2011).
- [23] H. F. Kay and J. L. Miles, *Acta Cryst.* **10**, 213 (1957).
- [24] P. H. Sun, T. Nakamura, Y. J. Shan, Y. Inaguma, and M. Itoh, *Ferroelectrics* **217**, 137 (1998).
- [25] H. Taniguchi, H. P. Soon, T. Shimizu, H. Moriwake, Y. J. Shan, and M. Itoh, *Phys. Rev. B* **84**, 174106 (2011).
- [26] Y. J. Shan, H. Mori, K. Tezuka, H. Imoto, and M. Itoh, *Ferroelectrics* **284**, 107 (2003).
- [27] W. Zhong and D. Vanderbilt, *Phys. Rev. Lett.* **74**, 2587 (1995).
- [28] V. F. Sears, *Neutron News* **3**, 26 (1992).
- [29] A. C. Larson and R. B. von Dreele, Los Alamos National Laboratory Report No. LAUR 86-748, 2000.
- [30] J. W. Sun, R. C. Remsing, Y. B. Zhang, Z. R. Sun, A. Ruzsinszky, H. W. Peng, Z. H. Yang, A. Paul, U. Waghmare, X. F. Wu, M. L. Klein, and J. P. Perdew, *Nat. Chem.* **8**, 831 (2016).
- [31] J. W. Sun, A. Ruzsinszky, and J. P. Perdew, *Phys. Rev. Lett.* **115**, 036402 (2015).
- [32] J. M. Tao, J. P. Perdew, V. N. Staroverov, and G. E. Scuseria, *Phys. Rev. Lett.* **91**, 146401 (2003).
- [33] H. J. Monkhorst and J. D. Pack, *Phys. Rev. B* **13**, 5188 (1976).
- [34] A. Togo, F. Oba, and I. Tanaka, *Phys. Rev. B* **78**, 134106 (2008).
- [35] A. Togo and I. Tanaka, *Scr. Mater.* **108**, 1 (2015).
- [36] S. Baroni, S. De Gironcoli, A. Dal Corso, and P. Giannozzi, *Rev. Mod. Phys.* **73**, 515 (2001).
- [37] G. L. Catchen, S. J. Wukitch, D. M. Spaar, and M. Blaszkiewicz, *Phys. Rev. B* **42**, 1885 (1990).
- [38] H. Moriwake, A. Kuwabara, C. A. J. Fisher, H. Taniguchi, M. Itoh, and I. Tanaka, *Phys. Rev. B* **84**, 104114 (2011).
- [39] D. Orobengoa, C. Capillas, M. I. Aroyo, and J. M. Perez-Mato, *J. Appl. Cryst.* **42**, 820 (2009).
- [40] A. M. Glazer, *Acta Cryst.* **B28**, 3384 (1972).
- [41] Z. M. Zhang, G. R. Lumpkin, C. J. Howard, K. S. Knight, K. R. Whittle, and K. Osaka, *J. Solid State Chem.* **180**, 1083 (2007).
- [42] A. A. Belik, S. Y. Stefanovich, B. I. Lazoryak, and E. Takayama-Muromachi, *Chem. Mater.* **18**, 1964 (2006).
- [43] K. S. Knight, *J. Alloys Compd.* **509**, 6337 (2011).
- [44] T. Y. Tan, B. J. Kennedy, Q. D. Zhou, C. D. Ling, W. Müller, C. J. Howard, M. A. Carpenter, and K. S. Knight, *Phys. Rev. B* **85**, 104107 (2012).